

# **Practical Course K2**

## **Luminescence of Quantum Dots**

# 1. Basics

The following figure (Fig. 1) shows the characteristic band structure of metals, semiconductors and insulators at a temperature of  $T = 0\text{K}$ .

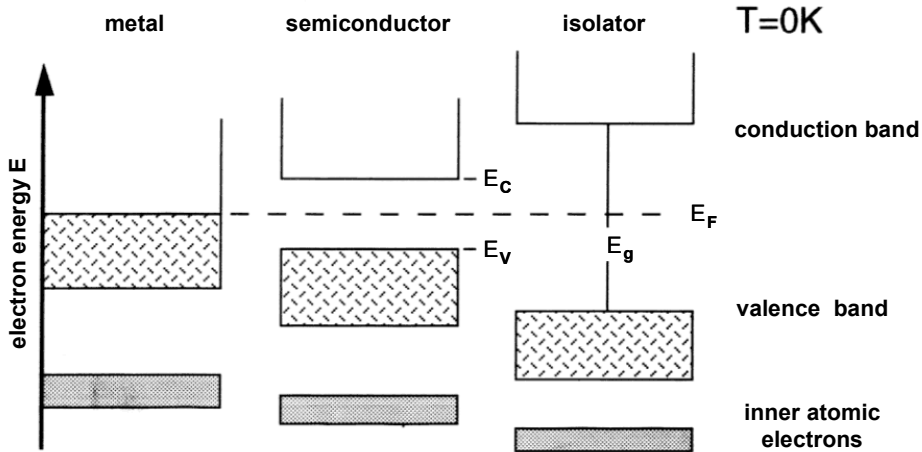


Figure 1: Band gap characteristics of different materials.

The **Fermi energy**  $E_F$  is the energy up to which the allowed electron states are occupied at  $T = 0\text{K}$ . The energetically highest band which is completely filled by electrons is called valence band, the lowest not entirely filled band is the conduction band. A fully filled band as well as an empty band does not contribute to electric conductivity. Such a material is called insulator. The energy difference between the upper edge of the valence band (called **valence band edge**  $E_v$ ) and the lower edge of the conduction band (called **conduction band edge**  $E_c$ ) is termed band gap  $E_g$ . In case of  $E_g < 5\text{eV}$  finite temperatures cause a thermal broadening which is determined by the **Fermi-Dirac distribution**  $f(E, T)$

$$f(E, T) = \frac{1}{\exp\left\{\frac{E - \mu}{k \cdot T}\right\} + 1}$$

where  $k$  is the Boltzmann constant and  $T$  is the absolute temperatur (Fig. 2).  $\mu$  is the chemical potential that is defined as the energy where  $f(E, T) = 0.5$  (with  $\mu(T=0) = E_F$ ).

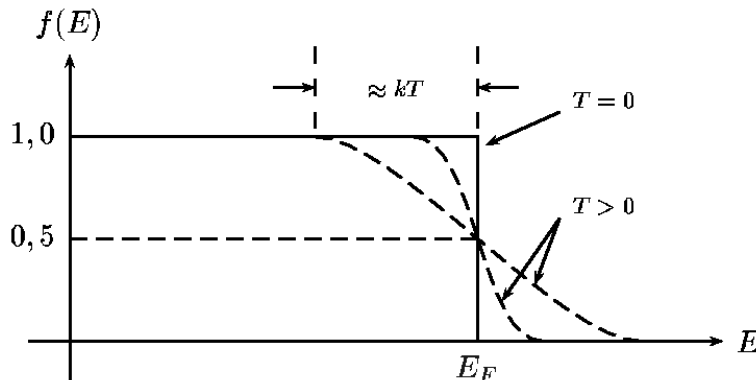


Figure 2: Fermi-Dirac distribution at different temperatures  $T$ .

Therefore statistically there is always a finite fraction of valence band electrons located in the conduction band at finite temperatures. In other words at finite temperatures there are thermally occupied states in the conduction

band. This activated electrons as well as the correspondingly created holes in the valence band contribute to electric current. Such a material is called semiconductor. Its electric resistance decreases with increasing temperatures (in contrast to metals).

Optical transitions are normally either **interband transitions**, between different energy bands, or **intra-band transitions**, within one band. They are characterized by a particle moving from an occupied to an empty state. Optical absorption is commonly referred to as interband transitions from the valence to the conduction band. Photon **emission** is mostly caused by transitions from the conduction to the valence band (**recombination**). This emission is also called **photoluminescence (PL)**.

In semiconductors or insulators photo emission is possible only above a certain energy corresponding to the band gap energy  $E_g$ . Below this energy the bulk material is optically transparent (referred to as **absorption edge**). Intra-band transitions often involve **phonon** interactions (a phonon is the quasi-particle of crystal lattice oscillations) and thus occur without photon emission. Hence intra-band transitions are commonly not observable in **photoluminescence spectroscopy**.

In a typical PL spectroscopy experiment the semiconductor is illuminated by monochromatic light with a photon energy above the bandgap ( $\hbar\omega > E_g$ ). Absorption within the material creates hot electrons and holes which quickly relax to the lowest energy states within the bands by phonon-phonon or electron-electron interaction (electrons relax to the lowest conduction band states, holes to the highest valence band states). The attracting electrostatic force can now lead to a bound state between an electron and a hole. This **electron-hole pair** is called **exciton**. The exciton lifetime of typically about 1ns by far exceeds the characteristic relaxation times (of the order of ps). Semiconductors show a direct bandgap if the bandgap energy is determined by conduction band and valence band states having the same k-vector and therefore being located at the same place of the Brillouin zone - see Fig. 3(b) below. In direct bandgap semiconductors exciton recombination is accompanied by strong luminescence.

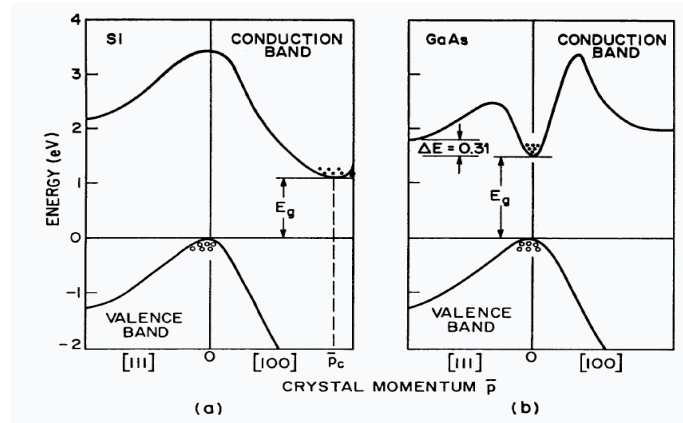


**Figure 3: Direct and indirect semiconductor band diagram.**

The energy of a radiated photon is exactly the difference between the band gap and the **exciton binding energy**. The electron-hole binding within the exciton is similar to that of the electron and proton of the hydrogen atom. Merely the screening of the electron-hole interaction caused by the surrounding crystal lattice with dielectric constant  $\epsilon$  has to be taken into account as well as the deviating particle masses within the crystal. Latter is accomplished by replacing the mass  $m$  by an **effective mass**  $m^*$  containing all the corrections imposed on the motion of electron and hole inside the semiconductor. Including this adjustments the calculations are identical to that of free particles. Hence for an infinitely large crystal in 3 dimensions the binding energy of the exciton ground state ( $n = 1$ ) is given by:

$$E_{Exciton} = \frac{m^* \cdot e^4}{8 \cdot \epsilon^2 \cdot \epsilon_0^2 \cdot h^2}$$

The following Fig. 4 schematically shows the exciton energy levels.

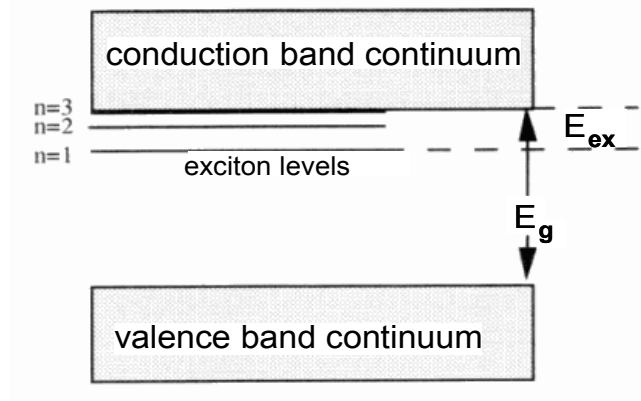


Figure 4: Exciton energy levels.

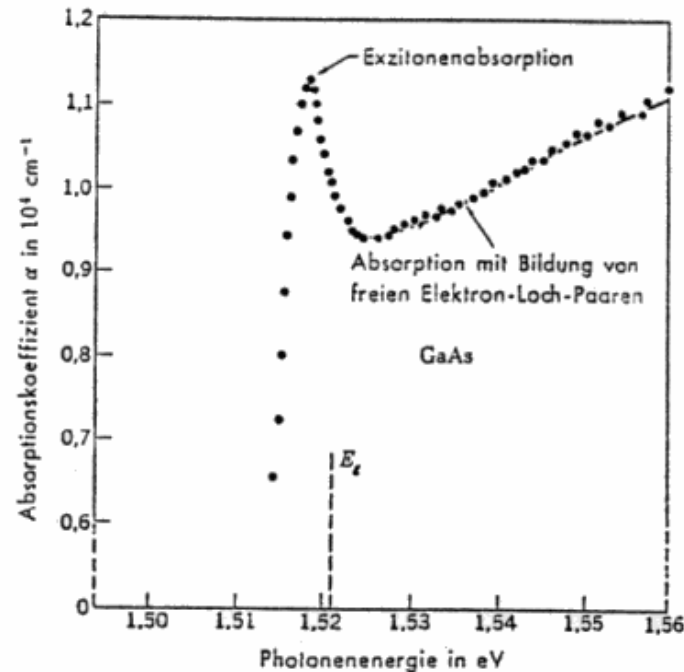
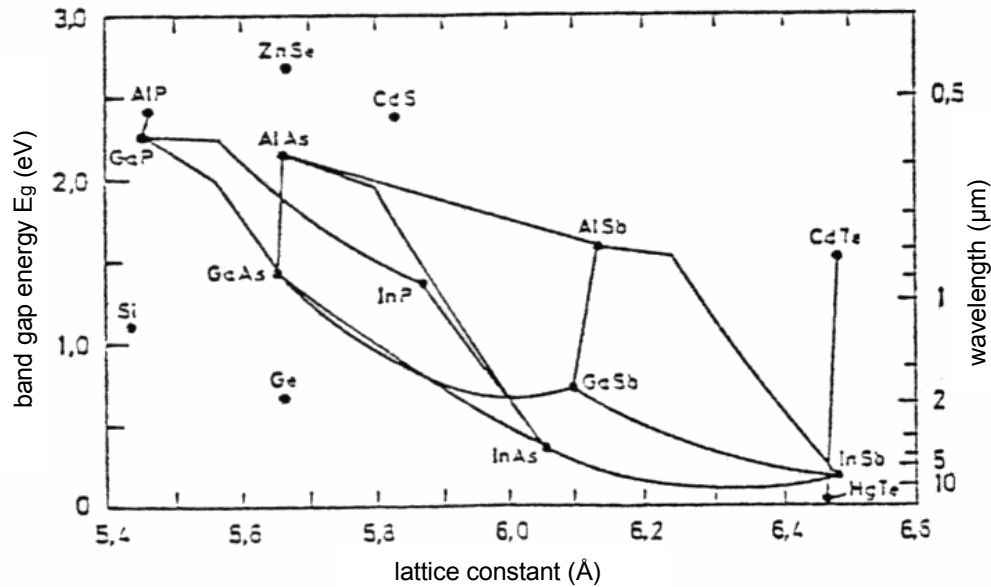


Figure 5: Optical absorption spectrum of a GaAs semiconductor at  $T = 21\text{K}$  containing a pronounced exciton absorption peak (Kittel, 1980).

## 2. Semiconductor heterostructures

By means of contemporary epitaxy methods like molecular beam epitaxy (MBE) or metalorganic chemical vapour deposition (MOCVD) it is possible to artificially deposit multiple layers of different single crystal (!) semiconductors on top of each other. The individual semiconductor layers can have different electrical properties, especially different band gap energies. Particularly III-V semiconductors (composed of elements of the 3<sup>rd</sup> and 5<sup>th</sup> main group elements of the periodic table) such as GaAs, InAs or InP are of main interest today (e.g. in semiconductor Lasers for DVD players, telecommunication, etc.). Furthermore this epitaxy methods allow ternary compounds too, e.g.  $\text{In}_x\text{Ga}_{1-x}\text{As}$ , whose band gap energies are located in between those of their binary components. Fig. 6 shows the band gap energy versus the lattice constant for the most common semiconductors and binary se-

semiconductor compounds at  $T = 300\text{K}$ .



**Figure 6: Resulting lattice constants and band gap energies for crystals made of common semiconductor compounds as well as crystals consisted of corresponding ternary combinations (Ibach Lüth, 1988).**

This dependency is particularly important since only semiconductors with equal or similar lattice constant can be epitaxially grown on top of each other without crystal defects. Larger differences in the lattice constants can lead to heavy stress within the crystal lattice which causes crystallographic defects like dislocations or defects. But smaller differences can already generate stress and with it changes of the electric potential. Fig. 6 also shows the resulting band gap or lattice constant of possible corresponding ternary compositions (lines). The resulting stack of different epitaxially grown semiconductor layers is called **semiconductor heterostructure**. Using appropriate epitaxy methods (e.g. MBE) the width of the transition region between adjacent layers can be only one single atomic layer. Consequently the bandgap change happens within only a few Å too. This yields the situation depicted in Fig. 7.

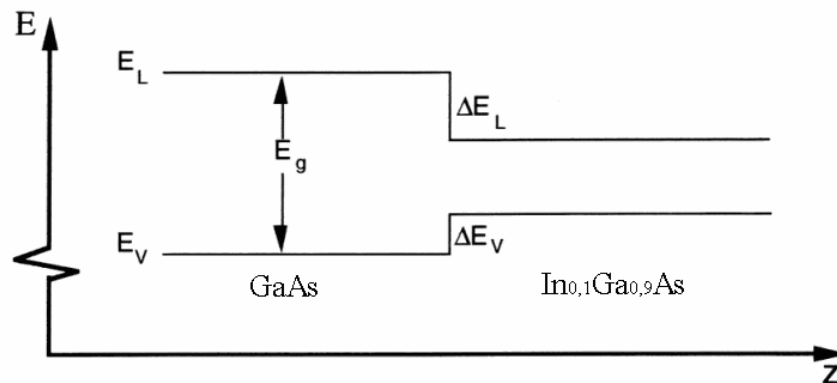


**Figure 7: Energy band diagram at the GaAs/InGaAs interface.**

Here the most important parameters which characterize the heterostructure are the **conduction and valence band discontinuity**  $\Delta E_C$  and  $\Delta E_V$ , respectively. Both depend on the particular semiconductor materials. E.g. in case of (stressed) GaAs/ $\text{In}_{0.1}\text{Ga}_{0.9}\text{As}$  the ratio is  $\Delta E_C/\Delta E_V \approx 60/40$ . If different materials are grown alternately the band-structure can yield a **quantum well** structure as shown in Fig. 8.

If free electrons (and holes) are now excited optically the charge carriers can relax quickly (typical  $10^{-11}$  s) and non-radiatively (due to phonon-scattering) into the lowest available energy states which are located inside the quantum well and form excitons. After the average exciton lifetime electron and hole recombine to release a photon of their corresponding energy difference (Fig. 8).

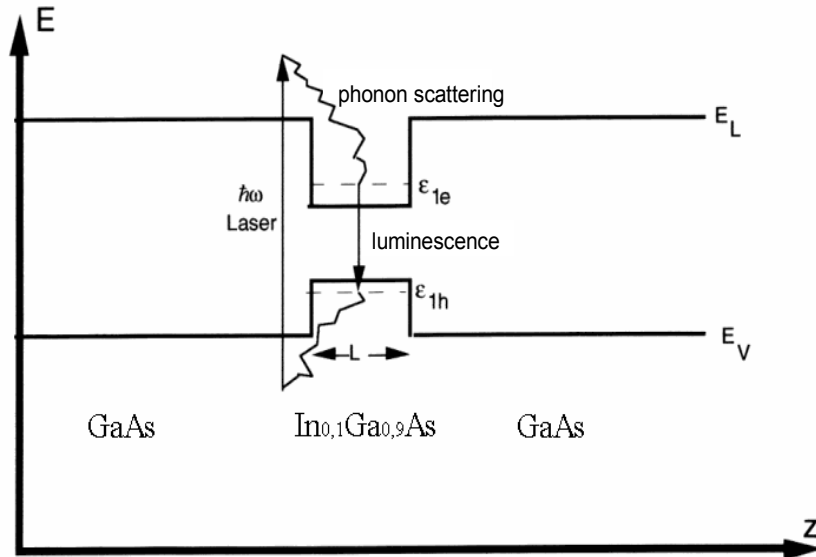


**Figure 8: Optical excitation, relaxation and luminescence within a quantum well structure.**

For electrons who are localized inside the quantum well quantum mechanical effects become important if the quantum well width  $L$  is small enough. It can be easily shown that quantum mechanical states inside the quantum well constriction become relevant if  $L$  is of the order of the electron de-Broglie wavelength (and similarly for holes inside the quantum well). Commonly denoting the heterostructure growth direction by 'z' it is called z-quantization. The z-quantization directly follows from the time-independent Schrödinger equation for an electron inside a crystal lattice which is confined in z yet free to move in the remaining two spatial directions.

### 3. Epitaxy methods

Particularly in present-day semiconductor physics or for electronic component technologies the ability of building up single crystal layers in a controlled fashion is essential. In order to study e.g. the Quantum Hall effect, multi-layer AlGaAs-GaAs heterostructure samples are commonly used. Semiconductor Lasers (e.g. quantum well Laser) or very fast transistors like High-electron-mobility transistors (HEMT) can be fabricated with this too. To build such layered semiconductor systems different epitaxy methods are available. They allow controlled growth with atomic precision in a controlled environment. Today the most common techniques for crystal growth on a substrate material are:

**molecular beam epitaxy (MBE)**

**metal-organic chemical vapour deposition (MOCVD).**

**metal-organic molecular beam epitaxy (MOMBE) or chemical beam epitaxy (CBE), respectively**

The basic principle of MBE (see Fig. 9) is to evaporate materials like indium, gallium or arsen before putting them on a substrate (e.g. GaAs). In order to avoid integration of defects or impurities the growth process is performed in ultra-high vacuum (UHV) at a pressure of  $p < 10^{-8}$  Pa. UHV chambers are made of high-quality steel as oxidization would highly increase the adsorption area. Turbomolecular pumps or ion pumps enable to produce and maintain such extremely low pressures which cause mean free paths of the vapoured gas molecules of the range of kilometers. Ion pumps ionize atoms by means of high electric fields and absorb them on appropriately charged electrodes using active metal films like titan. Turbomolecular pumps achieve the very low pressures by momentum exchange between the gas molecules and the blades of the rapidly rotating turbine wheels. To further decrease the remaining gas pressure the UHV chamber contains an internal liquid nitrogen cooling shield which freezes out chemical impurities.

The substrate material, e.g. a GaAs wafer, is attached to a substrate holder which is positioned in the centre of the UHV chamber. The holder is rotating while evaporation to allow more homogenous growth across the whole substrate. To avoid atoms or molecules to be attached exactly at the place where they reach the substrate it is heated up to about 500 to 600 °C. This yields sufficient high surface mobilities so that the incident atoms or mo-

olecules can distribute across the sample surface and built up a homogenous lattice structure. The atoms or molecules are delivered by effusion cells. Within the cell the underlying material, such as solid Ga or solid As in case of GaAs epitaxy, is evaporated by electric heating out of a boron-nitride crucible. The rate of growth on the substrate depends on the particle flow from the effusion cell and is therefore determined by the temperature of the crucible. The beam of atoms or molecules directed to the substrate is switched on and off by opening and closing mechanical shutters. The elaborate control of shutter opening and closing times and the crucible temperature is commonly done by computers. This is the only way to enable growth of heterostructures with atomic precision like multi-lattices serving as electrostatic charge barriers or  $\delta$ -doping layers. Especially ternary or quaternary alloys with exact compositions require accurate controls by a computer software.

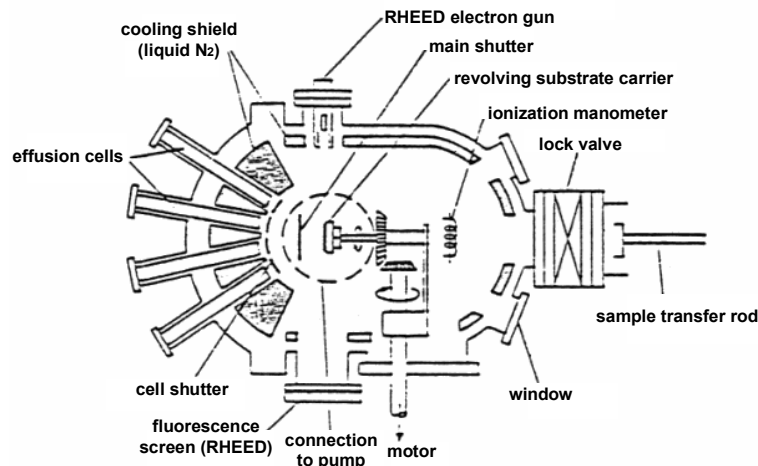


**Figure 9: Schematic of a UHV chamber for molecular beam epitaxy (MBE) of III-V semiconductor layers (Ibach Lüth, 1988).**

On the contrary homoepitaxy of e.g. GaAs layers on a GaAs substrate doesn't demand precise controls of the molecular or atom beam. For instance in case of GaAs at appropriate growth temperatures the growth rate is limited by the impact rate of Ga as the adhesion coefficient of As is close to 1 at an excess of Ga and close to 0 in case of absence of Ga. Therefore GaAs homoepitaxy is most efficient at As abundance. If As is involved it is furthermore important that the evaporated gaseous As beam mainly contains  $As_4$ -molecules which have to be cracked up thermally at the hot substrate surface before being able to contribute to the As growth process.

If doping is desired in case of III-V-MBE Si typically serves as n- and Be as p-dopant which are evaporated in effusion cells too. Switching on and off the corresponding shutters allows selective integration of the functionalized impurities.

The MBE machine is additionally equipped with an electron gun and a fluorescent screen to monitor the electron diffraction pattern (Reflection High Energy Electron Diffraction, RHEED). The diffraction pattern reveals the crystallographic structure of the grown surface. Furthermore the UHV chamber contains an ionization gauge which precisely measures the pressure inside the chamber as well as the flow of the particular atom or molecular beam.

The main advantage of the MBE method is its very short switching time (clearly below 1s) between different effusion cell sources due to the very low operating pressure. A typical growth rate of 0,3 nm/s, which corresponds to the depositions of about 1 monolayer per second, thus allows epitaxy with atomic precision. On the other hand the necessary UHV conditions impose the disadvantage of high costs for building up and operate the MBE as well as potential susceptance to failure.

Another important epitaxy technique is the metal-organic chemical vapour deposition (MOCVD). Here the gaseous materials are directed via gas flow controllers to a reactor made of quartz (see Fig. 10). In contrast to MBE during MOCVD the growth of a crystal happens by complex chemical reactions. In order to grow e.g. GaAs usually  $AsH_3$  and the metal-organic gas trimethylgallium (TMG) is used. There are further gas feeding pipes that allow growth of ternary alloys and incorporate the possibility of doping the growing material. Hydrogen is often used as a carrier gas for TMG and serves as purging gas for the whole system as well. The substrate (e.g. a wafer) is located on a quartz susceptor within the reactor. From the passing gas flow the target molecules diffuse to the heated substrate surface. By collisions within the gaseous phase as well as right at the substrate surface chemical reactions occur which release the actual target materials. After the aimed surface reactions have happened the unwanted reaction products diffuse away from the substrate surface back into the passing gas flow. The unused

materials such as reaction products are pumped off the reactor at the gas flow outlet side. They are injected into an oven which chemically breaks apart the dangerous components.

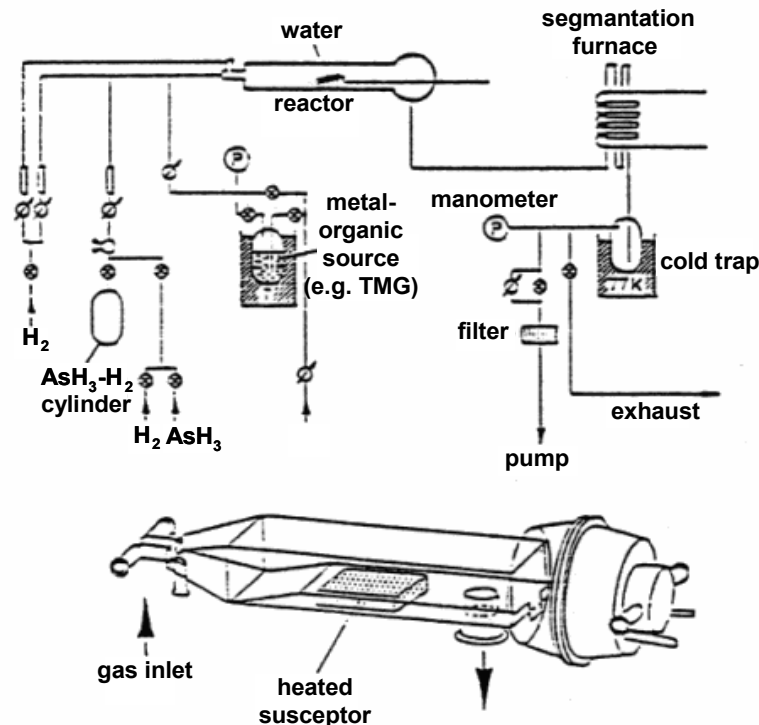


**Figure 10: Schematic of a metal-organic chemical vapour deposition (MOCVD) complex of III-V semiconductor layers. The upper part shows the overall overview, below the quartz reactor is depicted (Ibach Lüth, 1988).**

Advantages of the MOCVD process are the possibility to work at standard ambient pressure and a typically 10 times higher growth rate compared to the MBE process. The latter on the other hand doesn't allow precision on the atomic scale. Working at pressures below ambient pressure (low-pressure MOCVD) and employing particularly designed gas valve controls in turn enables shorter switching times between different materials and therefore allows the growth of heterostructures with atomically sharp defined material transitions.

A third commonly used epitaxy method is the metal-organic MBE (MOMBE) or sometimes referred to as chemical beam epitaxy (CBE). As MBE the MOMBE process works at UHV conditions. The source materials are gases which are injected in the reactor via pipelines and regulated valves. Here specifically designed gas intake constructions (capillaries) are used to form the molecular beam and to direct it to the substrate surface. Before entering the UHV chamber the gas must be pre-dissociated thermally within the capillary since this is not accomplished by collisions in the very low pressure environment of the chamber itself.

## 4. Quantum dots

Semiconductor heterostructures draw attention for quite some time as they allow to investigate studies of quantum mechanical effects in low-dimensional systems. Particularly in zero-dimensional systems electrons or holes can be localized at predetermined sites. A so-called quantum dot (QD) is one example of a zero-dimensional system. Incident Laser photons generate excitons within a semiconductor. Due to the resulting potential landscape the excitons are able to accumulate in the QDs. Afterwards the excitons can recombine by emission of photoluminescence light of corresponding wavelengths which contains information about the discrete energy levels of the quantum dots.

### 4.1. Fabrication of quantum dots

Growth of different single crystal layers with different lattice constants on top of each other leads to stress within the layers. There are two possible growth processes depending on the deployed material systems. In case of hetero-epitaxy of different materials on top of each other the growth process is dictated by the interplay of the dif-

ferent boundary surface and surface enthalpies:

$$\Delta\sigma = \sigma_E + \sigma_B - \sigma_S$$

where  $\sigma_E$ ,  $\sigma_S$  and  $\sigma_B$  are the specific free enthalpies of the epitaxy layer (E), the substrate (S) as well as the boundary surface (B) between the substrate and the epitaxy layer.  $\sigma_B$  predominantly contains the energy referring to stress. Depending on the sign of  $\Delta\sigma$  three different growth processes are possible:

- The **Frank-van-der-Merwe process** which refers to pseudomorphic growth of a layer. Here  $\sigma_S$  dominates and the growing layer fully and homogeneously coats the substrate. Additionally pseudomorphic stress builds up if the lattice constant of the epitaxy layer differs from the one of the substrate.
- The **Volmer-Weber process**: Here the enthalpies of the epitaxy layer  $\sigma_E$  and/or of the boundary layer  $\sigma_B$  dominate the growth. Virtually no coating occurs at all. Instead 3-dimensional growth takes place immediately, originating from different sites.
- The **Stranski-Krastanow process**: The growth starts as in case of the Frank-van-der-Merwe process, completely coating the substrate as  $\sigma_S$  dominates. However with cumulative thickness of the stressed epitaxial layer the boundary surface enthalpy  $\sigma_B$  is increasing too. This can result in a change of the sign of  $\Delta\sigma$  if a critical thickness  $h_{\text{CRIT}}$  is reached. Then a change to a Volmer-Weber-like growth takes place and 3-dimensional growth sets in (Fig.11).

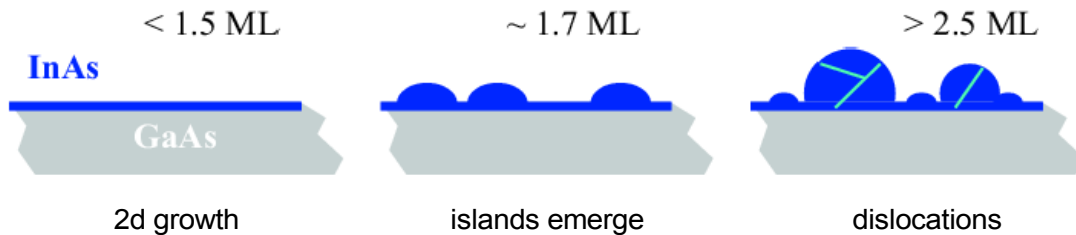


**Figure 11: Quantum dot growth.**

The Stranski-Krastanov process is often used to fabricate QDs in semiconductor heterostructures. As the final QD locations are not controlled in the general process the term self-assembled QDs is used.

For this practical course a sample is utilized which contains self-assembled InAs-islands grown on GaAs substrate layers. The sample was fabricated by A. Badolato at the UC Santa Barbara and was made available to us with best thanks. It includes the following layer sequence (see Fig. 12 as well):

- Substrate: (100) GaAs wafer + 2000 nm of grown GaAs
- Back contact: 20 nm n+ doped GaAs
- Tunnel barrier: 25 nm GaAs
- Quantum dots: 2 nm InAs
- Capping layer: 25 nm GaAs
- Tunnel barrier: superlattice of 29 times alternating AlAs und GaAs, each of thickness 2nm
- Capping layer: 4 nm GaAs
- Gate: 5 nm NiCr

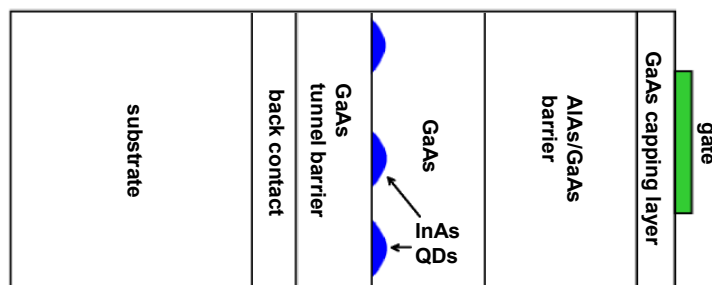


**Figure 12: Heterostructure of the sample.**

The critical layer thickness  $h_{\text{CRIT}}$  is about 2 monolayers (ML) in case of InP on top of GaAs. The resulting QDs are randomly distributed over the whole sample surface. The QD density of typically  $1 \cdot 10^9 \text{ cm}^{-2}$  can be evaluated with the aid of an atomic force microscope (AFM) or via a scanning electron microscope (SEM). The mean height and width of a QD are 2 nm and 40 nm, respectively. Due to their electronic properties QDs behave like zero-dimensional potential wells for charged particles. The resulting energy level scheme is therefore very similar to the energy level distribution of an atom. One aim of this practical course is to directly measure the basic level scheme of self-assembled QDs. After the QD growth process a thin layer remains between the QDs which is called wetting layer.

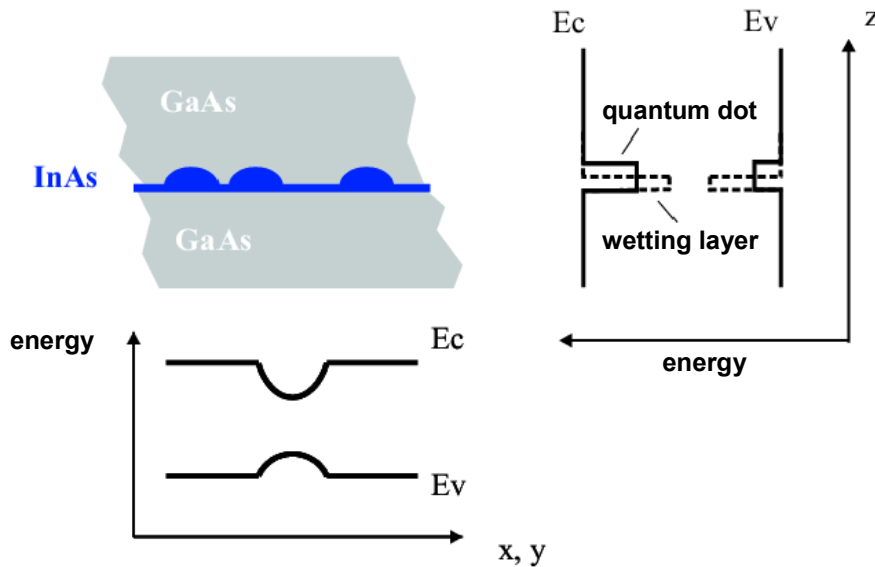


Figure 13: Band diagram of self-assembled quantum dots.

#### 4.2. Shape of the electrostatic potential

A schematic of the band structure of the used sample is shown in Fig. 14.

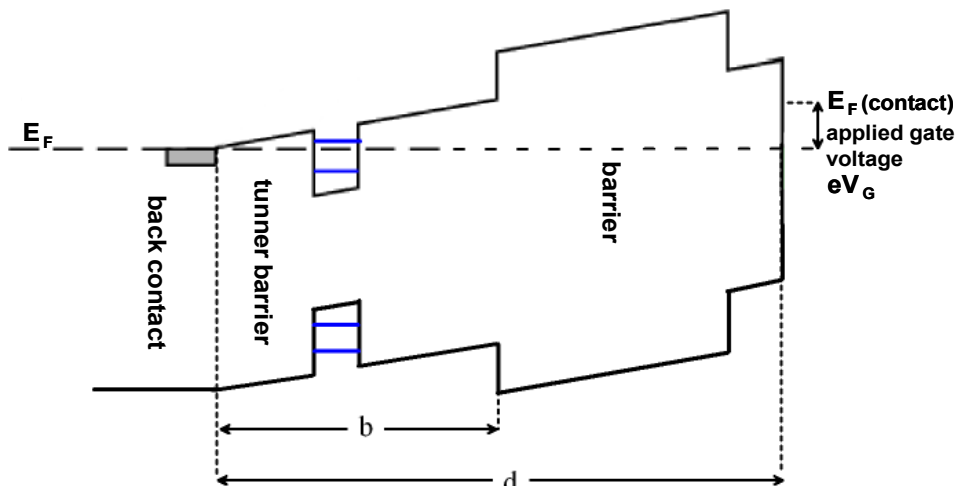


Figure 14: Band structure at applied external voltages.

The conduction band edge of InAs is located energetically below the GaAs conduction band edge. For the valence band edges the positions are reversed. Consequently the InAs bandgap is smaller than the bandgap of GaAs

which leads to a quantum well (QW) structure for the InAs layer sandwiched between GaAs sections. Excitons which are created in the vicinity of the QW will predominantly relax into the QW (see below) due to the lowered potential there. In the picture above  $d$  is the length of the so-called lever arm which on the right hand side is raised or lowered with respect to the Fermi energy as the applied gate voltage is decreased or increased, respectively. By tuning the gate voltage, the energy levels of the QW are shifted with reference to the Fermi level as well. Therefore this allows the controlled filling or depopulation of the different QW states.

### 4.3. Eigenstates of the quantum dot

In order to calculate the energy of the electron and hole states within the zero-dimensional QD confining potential the following simplifications are included:

- Due to its shape the QDs can be assumed to be effectively 2-dimensional. The ratio of height and lateral width is 2 nm / 40 nm. Hence it is possible to separate the corresponding wave functions by using the adiabatic approximation.
- The shape of the potential in xy-direction can be approximated by a parabolic function.
- Dot-dot interactions can be neglected. This is justified by the fact that the characteristic distance between two dots is about 300 nm at a typical dot density of  $1 \cdot 10^9 \text{ cm}^{-2}$ .

Thus the wave function of the z-component can be separated from the wave function of the xy-directions. Including the above assumption regarding the lateral potential, this leads to the Hamiltonian for a harmonic oscillator:

$$H = (p_x^2 + m^* \omega^2 \cdot q_x^2) / (2m^*) + (p_y^2 + m^* \omega^2 \cdot q_y^2) / (2m^*)$$

For a potential which exhibits rotational symmetry the angular momentum operator

$$L_z \equiv 1/\hbar (q_x p_y - q_y p_x)$$

can be defined. With  $H$  it generates a set of commuting operators. The solution of this problem are eigenstates  $\psi_{nm}$  with eigenvalues  $n=0,1,2,\dots$ , and  $m=-n,-n+2,\dots,n$ .

For example, the eigenfunction for an electron in the s-state  $\psi_{00}$  is:

$$\psi_{00}(\mathbf{r}) = (\pi l_e)^{-1/2} \exp(-\mathbf{r}^2 / (2 l_e^2)) \quad ,$$

with  $l_e$  and  $l_h$  the so-called effective lengths for electrons and holes.

An important implication are the resulting selection rules for each eigenfunction: The transition from an electron- to a holes state is only allowed for identical principal quantum number  $n$  of the initial and final state (Fig. 15). Therefore only transitions from a s-state to a s-state, p-p etc. are possible. In the optical response of the system only those transitions are observed. Mixed transitions (s-p, p-d, etc.) are strongly suppressed. The radiation is emitted isotropically. One aim of this practical course is to relate measured QD spectra to those transitions and to determine the corresponding transition energies.

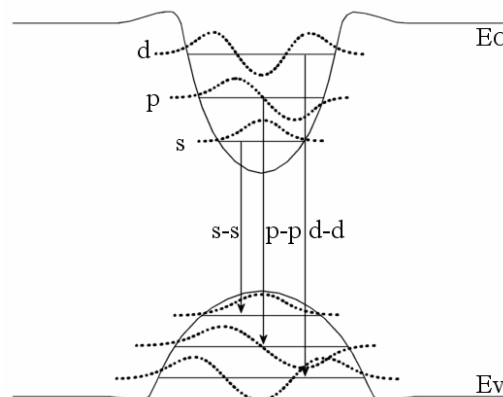


Figure 15: QD interband transitions.

#### 4.4. Origin of the photoluminescence

Illuminating the sample with light of energies larger than the band gap of the semiconductor material creates free electrons in the conduction band leaving holes in the valence band. Electrons and holes can lose energy by phonon interactions and relax to the lowest possible energy states where they can form a bound state of electron(s) and hole(s) called exciton. After a mean lifetime the exciton's electron can recombine with its hole radiatively. The energy of the emitted photoluminescence light is equal to the difference of the energies of the consisting charged particles minus their exciton binding energy.

#### 4.5. Exciton binding energy

In this section an expression for the exciton ionization field  $\vec{E}_i$  is derived which acts contrary to the binding force between the composing electron and hole. An externally applied electric field  $|\vec{E}_{\text{ext}}| = V_G / d$  between the gate on top of the sample and the backgate will break apart the exciton if it is higher than the attracting field between the exciton constituents. In this case electrons and holes can tunnel to the respective gate electrode building up a leakage current. It has to be taken into account that the particular sample of this practical course contains a blocking barrier for holes (Fig. 14). Accumulating charges there will create an electric field opposite to the external field. If the external electric field is much smaller compared to  $\vec{E}_i$  electrons and holes are able to energetically relax into the potential wells of the QDs and recombine later. For the electric field in the semiconductor  $\vec{E}$  the following approach is used:

$$\vec{E}_z = \left( \frac{V_G}{d} + E_{\text{int}} \right) \vec{e}_z$$

where  $V_G$  is the voltage between the top- and back-gate and  $E_{\text{int}}$  is the intrinsic electric field inside the semiconductor, acting at the QD plane. Furthermore,

$$E_{\text{int}} = -\frac{\Phi_{\text{pinning}}}{d} + E_{\text{hv}} = -\frac{\Phi_{\text{pinning}}}{d} + \frac{V_{\text{hv}}}{b}$$

with  $\Phi_{\text{pinning}}$  being the potential pinned with respect to the bandgap energy ( $E_g$ ) and  $V_{\text{hv}}$  being the opposite field potential which is generated by the optically induced holes which are stored at the blocking barrier.  $b$  corresponds to the distance between backcontact and blocking barrier where  $V_{\text{hv}}$  is acting (Fig. 14).  $V_{\text{hv}} / b$  can be neglected in case of comparatively low excitation powers (as used in the laboratory). Furthermore the following expressions are used:

$$e \cdot \Phi_{\text{pinning}} = \beta \frac{E_g}{2}$$

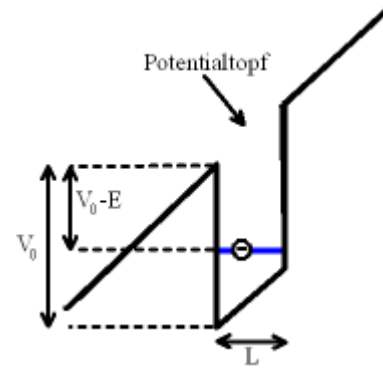
with  $\beta$  permitting a adjustable pinning potential w.r.t the middle of the bandgap energy ( $= E_g/2$ ). For GaAs as well as each intrinsic semiconductor  $\beta$  equals 1. The bandgap of GaAs is  $E_g = 1,520$  eV (equals a wavelength of 817 nm). The pinning potential is therefore located right in the middle of the bandgap. The result is:

$$E_z \approx \frac{V_G}{d} - 1 \cdot \frac{E_g}{2e \cdot d} = E_i$$

#### 4.6. Estimation of the tunnel barrier height

By applying a sufficiently high gate voltage excitons are separated and the remaining charges are pulled to the respective gate electrodes. If the charge carriers are located within the QDs they must tunnel through the potential barrier in order to get to a gate. The WKB method (which can be derived from the Fowler-Nordheim equation) yields a sensible estimation of the transmission amplitude and the corresponding transmission coefficient  $|T|^2$ :

$$|T|^2 \cong \exp\left(-\frac{4\sqrt{2}}{3} \frac{\sqrt{m}}{\hbar} \frac{(V_0 - E)^{3/2}}{e \cdot |E_i|}\right)$$



$|T|^2$  is the probability for an impinging particle to tunnel through a potential barrier. The semiclassical electron is supposed to move back and forth in a quantum well of length  $L$ . For the ground state ( $L = \lambda/2$ ) the momentum of the electron is given by

$$p = \hbar k = \hbar \frac{2\pi}{\lambda} = \hbar \frac{\pi}{L}$$

This allows to calculate the time the particle needs to travel from one QW barrier to the opposite one and back ( $2L$ ),

$$t = \frac{2L}{p/m^*} = \sqrt{2}L \sqrt{\frac{m^*}{E}}$$

The reduced mass of the electron is  $m^*$ . The particle needs roughly  $1/|T|^2$  barrier hits in order to leave the QW.

Thus the corresponding life time  $\tau = t/|T|^2$  till the tunnel process has been occurred is:

$$\tau = L \sqrt{\frac{2m^*}{E}} \exp\left(\frac{4\sqrt{2}}{3} \frac{\sqrt{m^*}}{\hbar} \frac{(V_0 - E)^{3/2}}{e \cdot |E_i|}\right)$$

The effective mass of the electron in GaAs is  $0,07 \cdot 9,1 \cdot 10^{-31}$  kg. The energy of an electron confined inside a QW is:

$$E = \frac{\hbar^2 \pi^2}{2m^* L^2}$$

## 5. Experimental setup

The luminescence setup (Fig. 16) mainly consists of five parts:

illuminating light source

imaging optics

sample holder hosting the sample

spectrometer

CCD detector plus read-out electronics and Computer

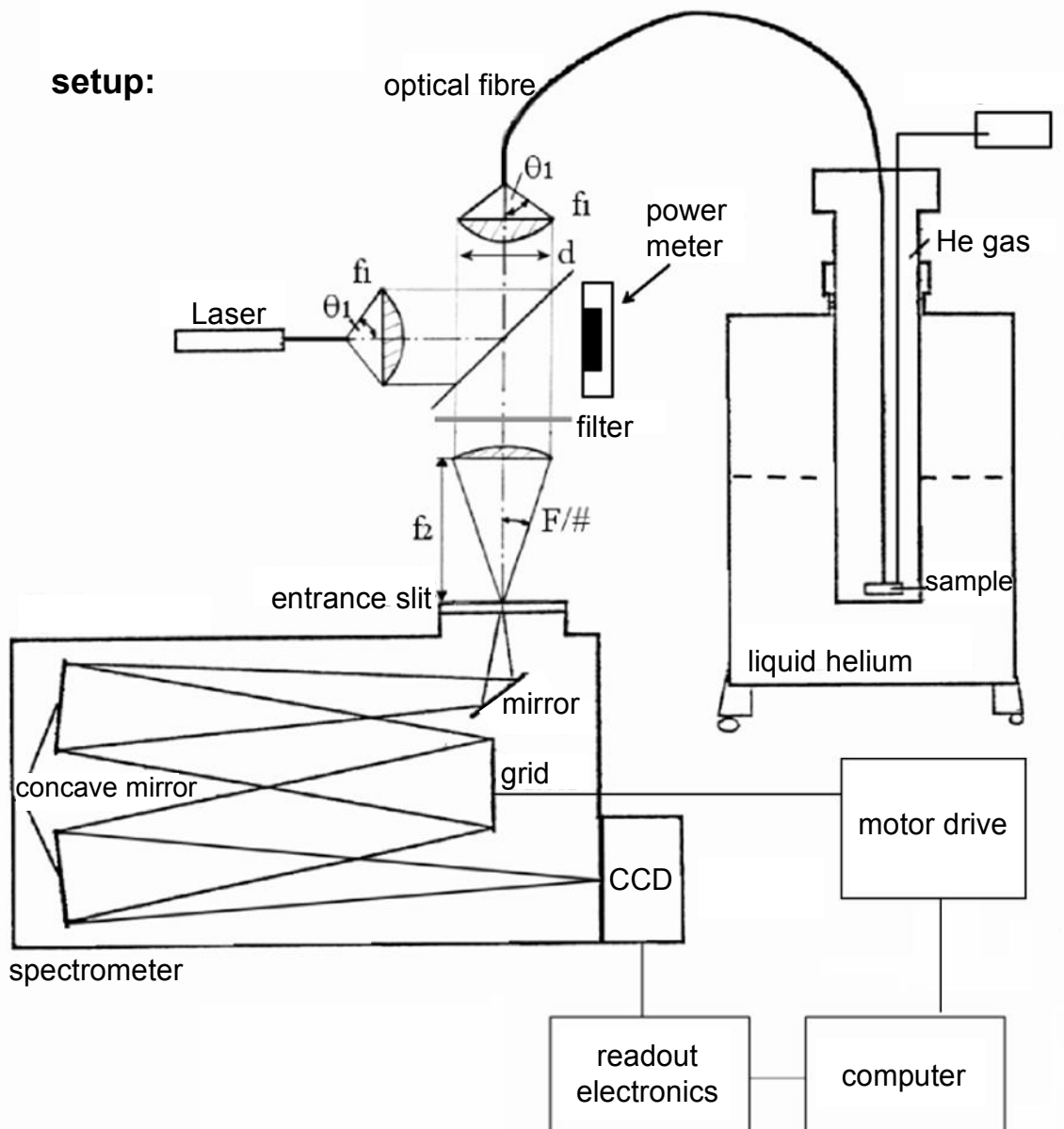


Figure 16: Experimental setup.

### Light source:

For the practical course a semiconductor laser ( $\lambda = 685\text{nm}$ ) is used. Utilizing a laser is necessary as its emitting light shows high spectral intensity at a well-defined emission energy. Additionally the laser radiation is emitted within a narrow solid angle. This allows to e.g. couple high emission intensities into an optical fibre. An optical longpass filter strongly suppresses laser light or scattered light at wavelengths below  $830\text{nm}$ . The filter is located right before the spectrometer entrance slit to protect the CCD detector. The intensity of the laser can be tuned by an adjustable screw positioned at the rear of the laser housing.

### Imaging optics:

The Laser emission is directly coupled into an optical fibre ( $N_A = 0,39$ ,  $N_A = \sin\theta$ ,  $\theta = \text{critical angle}$ ). The light leaving the fibre on its opposite end is collimated by a lens to a beam of about 20 mm in diameter. After passing a beamsplitter (of reflectivity 50%) the laser light is coupled into a second identical optical fibre leading to the sample. The sample is located in an elongated metal tube which is actually cooled down for the lab course experiment. The excitation light is coupled into a third fiber that is fixed within the cooled setup part and which terminates close above the sample surface (Fig. 17). The luminescence response of the sample is partly coupled into the same fibre end and propagates back through the same optical beam path. The luminescence which passes the beamsplitter straight-lined is focused onto the spectrometer's entrance slit by another optical lens. The F-number ( $F/\# = \text{focal length}/\text{diameter}$ ) of the spectrometer is 4.2 ( $= 1/(2N_A)$ ). The angle of aperture of the light cone which passes through the entrance slit of the spectrometer must not exceed a critical value in order to fully hit the subsequent internal spectrometer mirror (Fig. 18). On the one hand this would imply signal intensity lost. On the other hand it can generate scattered light which can cause a rising CCD background level or artefacts of the CCD output signal.

### Sample holder and sample:

The sample ( $3 \times 5 \text{ mm}^2$ ) which is glued on a Aluminium sample holder is placed close ( $< 1 \text{ mm}$ ) to the polished end of an optical fiber (Fig. 17). The sample holder is located in a tube-shaped housing which was evacuated and thereafter filled with helium gas under low pressure. The latter generates thermal contact between the sample and the tube housing which is cooled by liquid helium.

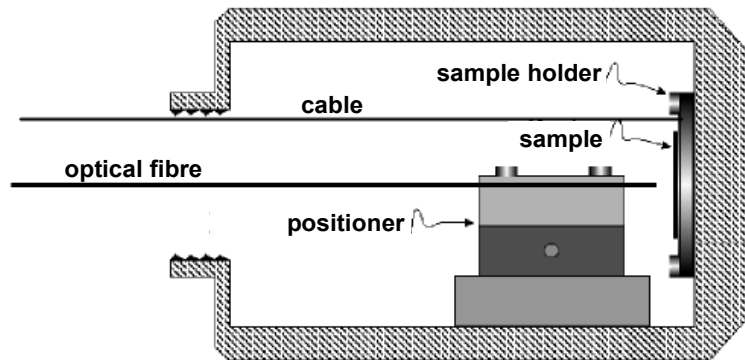


Figure 17: Sample holder and sample.

### Optical spectrometer:

A schematic view of a typical spectrometer is shown in Fig. 18.

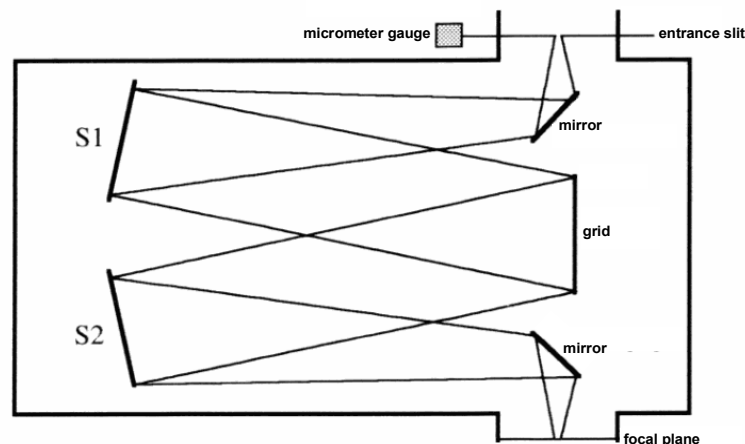
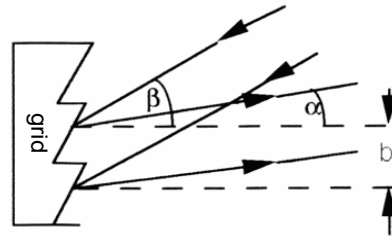


Figure 18: Optical beam path of a spectrometer.

The light source which is investigated by the spectrometer (in this case the fibre end) is focused by a lens (Fig. 16) on the entrance slit of the spectrometer. The width of the slit opening is adjustable with the aid of a micrometer screw ( $10\mu\text{m} / \text{Skt}$ ). The slit is located right at the focal length of the spherical mirror S1 that collimates the incoming light and directs it to the diffracting grid. The focal length of each spherical mirror is 320 mm. The employed grid has a lattice constant of 1200 lines per mm, a reciprocal linear dispersion of  $1.9 \text{ nm/mm}$  and can be used in the wavelength range of 500 - 1100 nm. The transmission of the spectrometer is 50%. The incident light is diffracted as shown in Fig. 19.



**Figure 19: Spectrometer grid deflection.**

This yields the situation depicted in Fig. 20.

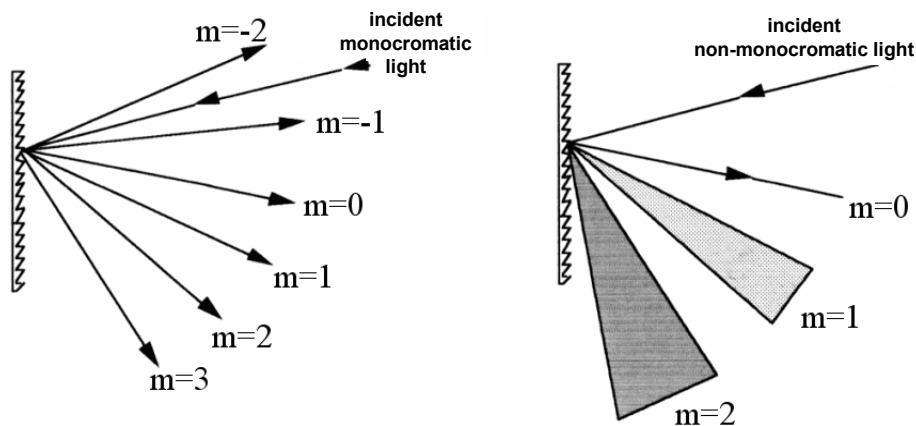


**Figure 20: Spectrometer grid deflection orders.**

In case of incident polychromatic light the actual lattice position determines the wavelength range which is deflected to the spherical mirror S2. The detector is located right at the focal length of S2. Normally the lattice is placed so that the diffraction of the first order ( $m=1$ ) is guided onto the detector. The higher order diffractions usually carry strongly decreased light intensity compared to the first order and consequently are virtually not useful experimentally. The lattice position can be adjusted by a screw by hand. The spectrometer used for the practical course setup has an available wavelength range of 500-1100nm.

For further spectrometer specifications, see appendix.

### CCD detector

For over 25 years the Charge Coupled Device (CCD) is a key component of optical detection. CCDs are detectors made from semiconducting n-p-doped silicon layers to which a grid of micro electrodes is attached (Fig. 21). A proper voltage applied to a micro electrode yields a quantum well potential structure below the electrode. Electrons generated by the photoelectric effect can be captured there. The read-out process involves a clocked change of the local potentials which can shift trapped charges in between adjacent potential wells. At the edge of the CCD detector the charge of each row is read out separately, electronically amplified and digitized by an A/D converter.

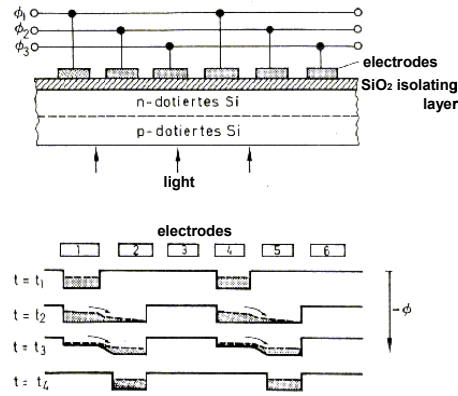


**Figure 21: Schematic of the working principle of a CCD detector.**

The main advantage of a CCD compared to a photo multiplier is the possibility of multiplexing. Every pixel of the CCD chip detects simultaneously without reducing spectral resolution or intensity as the entrance slit is imaged onto the detector. Typical widths of the slit window are in the range of 10-20  $\mu\text{m}$  which is about the size of each CCD pixel. In case of using a photo multiplier it would be necessary to adjust the width of the beam exit aperture to the same size too in order to avoid decline of spectral resolution. And on the other hand operating with a CCD device gains intensity since it features an increased quantum efficiency. Nowadays photomultiplier are predominantly used if high temporal resolution is required which a CCD cannot deliver without additional technical aid<sup>1</sup> due to the quite time-consuming read-out process (milliseconds).

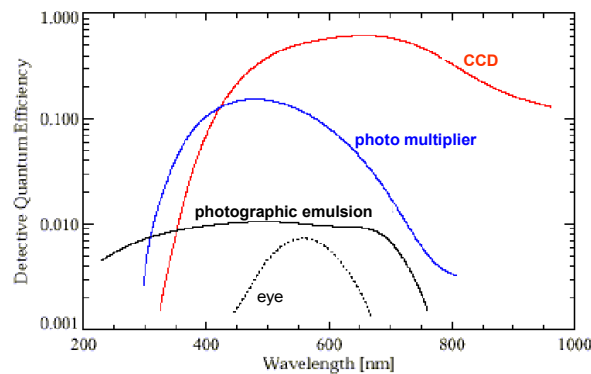


**Figure 22: Sensitivity of different detectors (QDE).**

The following obstacles have to be taken into account using a CCD detector device:

- All charge-controlled detectors must be cooled in order to minimize thermal noise. Typical target temperatures for spectroscopy applications are in the range of 140 - 160 K. If it would be cooled down further the relative sensitivity would drop as well which would only allow to detect sources of higher luminosity (e.g usage in cameras).
- Additionally to thermal noise the signal is affected by noise emerging from the read-out process of the amplifier. However there has been achieved significant progress eliminating this noise contribution so that it is negligible nowadays.
- The doping of the detector cannot be flawless in either case. Thus a CCD chip can always contain defective pixels which lead to signal loss even if the read-out process would have an efficiency of 100%. Even whole pixel lines can be defective. Those pixels are damaged permanently.
- Images aquired with long integration times can particularly be distorted by so-called spikes which result from strong local electric charge accumulation within CCD pixels. The cause can be natural radioactivity in particular glasses used for the devices or cosmic radiation originating from collisions of high-energy particles from space with molecules of the earth's upper atmosphere („cosmics“). Spike events may be compensated by redundant data accumulation.

<sup>1</sup> There are particular CCD detectors including a microchannel plate detector connected ahead which allow temporal resolutions up to 300ps.

The cooled CCD camera which is attached to the spectrometer has a resolution of  $1024 \times 256$  pixels. The edge length of each pixel square is  $27 \mu\text{m}$  yielding a total photo-sensitive area of  $27,6 \times 0,69 \text{ mm}^2$ . In order to measure one (1d) spectrum each final pixel information can stem from all 256 vertically stacked pixels of the chip (called 'binning' of the chip) which enhances the signal-to-noise ratio. For instance in case of purely white noise it would be increased by a factor of  $\sqrt{256} = 16$  as the mean signal increases by a factor of 256 in contrast to a fluctuation amplitude gain of 16. The possible maximum number of electrons storable in one potential well till leakage to adjacent wells occurs is crucial for the dynamic range of a camera. In case of horizontal read out the capacity of the read-out register is essential which typically is  $10^5$  electrons. A high-efficiency CCD as used in this practical course costs about 30.000 € ! The CCD chip is located in the focal image plane of the spectrometer whereby a minimal line width of around 3 pixels is attained. At 800 nm the total wavelength range of a single spectrum is hence 50 nm.

The chip is cooled via liquid nitrogen (boiling temperature at ambient pressure: 77.4 K) and additionally heated to reach the optimal operating temperature. The controller of the CCD camera serves as temperature controller too. A full filling leaves a cooled down camera cold for about 6 hours.

The total camera noise  $N$  consists of three parts and can be written as

$$N^2 = N_R^2 + N_D^2 + N_S^2.$$

$N_R$  is the read-out noise emerging while reading out and amplifying the charge signal of each camera pixel. For the used camera here it is 2 counts per read out per line.  $N_D$  is the noise level by the dark current that occurs as even without incident photons charges can be accumulated in each pixel. Finally  $N_S$  is the noise of the measured signal itself (Photons obey Poisson statistics). The dark current decreases exponentially with decreasing temperature. At 77.4 K it is less than 1 electron per hour and pixel and thus  $N_D$  can be neglected here.

The camera has a quantum efficiency of about 0.4 for the incident wavelength range of 600nm bis 900nm. So a detected single event results from 2.5 photos on average.

### **Read-out procedure**

The read-out electronic circuit acquires every single spectrum (intensity versus pixel number) from the CCD chip one by one. Intrinsically no information regarding the actual wavelength is delivered. This must be executed afterwards using the so-called mid pixel number which refers to the particular pixel (line) of the CCD chip where the wavelength which was set at the spectrometer is incident.

## 6. Experiment

1. Build up the experimental setup and make yourself familiar with the spectrometer control and the software. Be careful while handling with the Laser! Even reflexes off plain metal surfaces (watches, rings, ...) are dangerous. You may use protection goggles. Additionally, available curtains should be closed in order to avoid further reflexes.
2. Calibrate the evaluation software by means of the optical spectrum of the neon lamp in the wavelength range of 800 nm to 850 nm (see the table of wavelengths of the neon spectrum below) using the mid pixel. It is recommended to use the highest peak at around 837.76 nm. After successful adjustment the mid pixel value should be maintained for all measurements.
3. Connect the glass fibre to the sample stick, shade the lab (switch off lights and close the curtain) and record a spectrum from the sample at  $T = 4.2\text{K}$  in the wavelength range of 775 nm to 975 nm at maximum Laser power (using the software CCD\_LittleSpec). In case the spectrum saturates use a correspondingly lower excitation power as maximum Laser power. Explain the origin of the each observed peak. CAUTION: Do not move the spectrometer range very close to ( $\sim 1\text{nm}$ ) or on the Laser wavelength! This can irreversibly damage the CCD detector (**!!! Laser wavelength = 685nm !!!**).
4. Using the measurement parameters of task 3., record one spectrum of the background signal (i.e. no sample, thus the fibre stays connected and the Laser is switched off) in the wavelength range of 775 nm to 975 nm in the darkened lab (closed curtain, respectively) as well as one spectrum in the lightened lab. What causes the differences of the spectra?
5. Connect the voltage source to the sample stick, + to connector 2 and - to connector 3. Set the excitation power to 10% of the maximum value chosen before (powermeter: ask adviser). First record one spectrum in the wavelength range of 920 nm to 970 nm <sup>(1)</sup> at  $V_{\text{GATE}} = 0\text{ mV}$  (integration time = 2000ms). The peak heights should reduce if  $V_{\text{GATE}}$  is decreased to  $-20\text{ mV}$ . If not, the gate connections are exchanged. Furthermore take spectra, using the same wavelength range, one for each  $V_{\text{GATE}} = -5, -10, -15, -20, -25, -30, -35$  and  $-40\text{ mV}$ .
6. Photoluminescence depending on excitation power: record 10 spectra in the range of 920 nm to 970 nm ( $V_{\text{GATE}} = 0\text{ mV}$ ) at different excitation powers in between 100% and 2% of the maximum power value chosen before. Determine the area below each of the two energetically lowest peaks by fitting two Gauss curves to the data (e.g. using the software OriginLab). Which conclusions can be drawn from the graph "peak curve area versus excitation power" ?
7. Further evaluation of the data: e.g. by using OriginLab, import the data and plot it. By using the menu "analysis" - "fitting" - "nonlinear fit" - "open dialog" two Gaussian distributions can be fit to the data. If the result is not satisfactory aforesaid "open dialog" box can be used for corrections. Plot the resulting area of the energetically lowest peak versus the applied gate voltage. Approximate the threshold value of the gate voltage (at which the peak would just vanish) by a linear fit procedure. Explain why the peak intensity drops while decreasing the gate voltage.
8. Estimation of the tunnel barrier height: calculate the ionisation field by utilizing the obtained threshold voltage. The tunnel barrier  $V_0$ -E can be derived from the equation for the recombination time. The recombination time can be assumed to be  $\tau = 1\text{ ns}$  here.

(1) corresponds to a spectrometer position of 948 nm.

## Literature:

- Ibach, Lüth: Festkörperphysik, Einführungen in die Grundlagen, Springer-Lehrbuch, 2. Auflage 1988, insb. Kap. 12.7  
Kittel: Einführung in die Festkörperphysik, Oldenbourg Verlag München Wien, 5. Auflage 1980

(or other books about solid state physics)

other sources: D. Haft: Diplomarbeit am LS Kotthaus, 1998

## © by

>> intruction initial (German) version:

Florian Bickel, 5/2001, Christoph Bödefeld, 2/2002

>> 2<sup>nd</sup> (German) version:

Udo Beierlein, 4/2004, Felix Mendoza, 2/2010 & 11/2010

>> English translation:

Enrico Schubert, 2/2015

## Appendix

### Neon spectrum (measured):

Wl_air / nm	E_Photon / eV	log_gf
703.2413	1.762780	-0.250
717.3939	1.728005	-1.310
724.5166	1.711017	-0.600
743.8898	1.666457	-1.150
748.8871	1.655337	0.047
753.5774	1.645034	-0.060
754.4045	1.643230	-0.441
794.3181	1.560660	-0.294
808.2457	1.533767	-2.210
811.8549	1.526949	-0.766
812.8911	1.525002	-1.404
813.6406	1.523598	0.072
825.9379	1.500913	-0.675
826.6077	1.499697	-0.045
830.0326	1.493509	0.014
837.7607	1.479732	0.669
841.8427	1.472557	-0.109
846.3357	1.464739	-2.776
849.5359	1.459222	0.425
854.4695	1.450796	-1.770
857.1353	1.446284	-1.271
859.1259	1.442933	0.062
863.4647	1.435683	-0.067
865.4383	1.432409	0.338
867.9493	1.428265	-0.304
868.1921	1.427865	-0.579
870.4111	1.424225	-1.330
877.1656	1.413258	-0.458
878.0621	1.411815	0.212
878.3753	1.411312	0.232
885.3867	1.400135	-0.259
886.5755	1.398258	-0.174
891.9500	1.389833	-1.026
898.8557	1.379155	-1.320

## Short introduction of the data evaluation with "OriginLab"

Open a worksheet: **file / new / worksheet**

Import data file: **file / import / single (or multi) ASCII**

Plot a graph: fully mark x column, e.g. A(x), and y column, e.g. B (y), than **plot / line / line**

Add further graphs to an already plotted graph: mark y column, e.g. B(y), of the new worksheet, move the cursor to the right edge of the column till the „Sine Graph“-symbol becomes visible, then click + hold left mouse button and draw the column directly into the desired (already plotted) graph (symbol must be shown again), by letting go the mouse button the additional graph has been added

"analysis" - "fitting" - "nonlinear fit" - "open dialog"

Gauss fits onto peaks: **analysis / fitting / nonlinear fit / open dialog** , Chose Gauss, at **settings / advanced / replica** the number of simultaneously fitted functions can be set. Than chose the max positions of the peaks. After successful fitting the data the refering fit parameter values can be find in a separate window in the folder section

Plot a graph from extracted areas: open a new worksheet, enlist area + corresponding error values and refering voltages or power values, **plot / symbol / scatter**

Linear fit: chose graph, then **analysis / linear fit / open dialog**

Export a graph: chose graph, then **file / export graphs / open dialog** , chose desired graphic format and select a proper target folder

## Additional information about the spectrometer

### Linear dispersion of the lattice

Depending on the exit angle adjacent deflected beams carry different phases with respect to each other which can lead to interference. Maxima occur if the optical path difference of adjacent beams equals

$$b (\sin \alpha + \sin \beta) = m\lambda \quad (A1)$$

where  $b$  is the lattice constant,  $\beta$  the angle of incidence,  $\alpha$  the exit angle and  $m$  the order. From A1 the angle dispersion of the lattice can be derived:

$$d\beta / d\lambda = m / (b \cos \beta) \quad , \quad (A2)$$

The linear dispersion in first order approximation in the focal plane of the spectrometer therefore results from the spectrometer focal length  $f$  as

$$dx / d\lambda = f (d\beta / d\lambda) = mf / (b \cos \beta) \quad . \quad (A3)$$

### Resolution of a spectrometer

The spectral resolution  $R = \lambda / \Delta\lambda$  is defined by the distance  $\Delta\lambda$  at which two neighbouring spectral lines can just be distinguished from each other. According to diffraction theory a lattice diameter  $D$  yields a maximal angular resolution of

$$\Delta\alpha = \lambda / D \quad . \quad (A4)$$

With  $d\alpha / d\lambda$  the maximum spectral resolution is thus

$$\Delta\lambda = b \cos \alpha (\lambda / mD) \quad , \quad (A5)$$

which yields:

$$R = mD / (b \cos \alpha) \quad . \quad (A6)$$

$N = D / b$  (total number of lattice bars). At small angles of dispersion  $\alpha$  it simplifies to  $R = mN$ .

Equation A6 illustrates the possibilities for enhancing the spectral resolution:

- observation in high spectral order  $m$  (but intensity drops dramatically!! -> unfeasible),
- enlargement of the lattice diameter  $D$ ,
- reducing the lattice constant  $b$ , or
- viewing at higher exit angles  $\phi$ ,

whereas the possibilities are restricted by the lattice equation (A1) and by technological limits ( $b$ ,  $D$ ). The best possible resolution is frequently not limited by the diffracting lattice though. In the experiment other inaccuracies are crucial. As the spectrometer images the entrance slit 1:1 onto the detector the final resolution is at least of the order of the slit width or, even worse, is determined by the spherical aberration of the focussing mirrors.